

REAL-TIME TRANSVERSE EMITTANCE DIAGNOSTICS*

P. Piot, G.A. Krafft, R. Li, J. Song

Thomas Jefferson National Accelerator Facility, VA23606 Newport News, USA

Abstract

With the increasing interest in high-brightness beams and the recent advances in photoemission guns capable of producing such high-charge, low-emittance beams, measuring transverse emittance has become a primary concern, especially in driver accelerators for free-electrons lasers (FELs) where a degradation of this parameter could result in significant deterioration of the FEL gain. Hence frequent and fast measurement are needed, particularly when detailed parametric studies are required. Commonly used methods include optical transition radiation (OTR) based methods and trace space sampling methods. We will discuss these methods and provide motivation for our method of on-line emittance measurement in the Jefferson Lab FEL.

1 INTRODUCTION

The characterization and measurement of transverse phase space is a longstanding topic widely discussed in the literature [1]. In this paper we concentrate on methods that provide an on-line measurement of emittance and Twiss parameters. We quantify "on-line" as an update rate of the order of a second. Throughout this paper the JLab FEL driver-accelerator is taken as an example. In this paper we use the root mean square (rms) emittance. For the $x - x'$ trace space it is defined as:

$$\bar{\epsilon}_x = \kappa \left[\langle (x - x_0)^2 \rangle \langle (x' - x'_0)^2 \rangle - \langle (x - x_0)(x' - x'_0) \rangle^2 \right]^{1/2} \quad (1)$$

where x and $x' = dp_x/dp_z = x/z$ are respectively the position and divergence coordinates. The $\langle \cdot \rangle$ designates the average operator on the two-dimensional trace space distribution $\rho_2(x, x')$, the constants x_0 and x'_0 are the first order moments in position and divergence. κ is a scaling factor; henceforth we set its value to 1 to conform to the Sacherer [2] definition of rms emittance. Another commonly used definition of rms emittance was defined by Lapostolle [3] and now referred to as the effective rms emittance, defined by letting κ be 4. In this paper we will also use the normalized emittance defined as $\bar{\epsilon}_x^n = \beta\gamma\bar{\epsilon}_x$. The advantage of considering an rms-type emittance is that its definition is not as arbitrary as it is for the geometric emittance commonly used by experimentalists (which is defined as the trace space area of a contour encompassing a certain fraction of the beam particles). The rms emittance also allows comparison of beam quality from different facilities. Finally the concept of rms emittance is a figure

of merit of the statistical properties of the beam since it is related to the beam entropy [4]. Along with the emittance, the trace space is also specified by the Twiss parameters that are related to the moments: $\alpha_x = -\langle xx' \rangle / \bar{\epsilon}_x$, $\beta_x = \langle x^2 \rangle / \bar{\epsilon}_x$, $\gamma_x = \langle x'^2 \rangle / \bar{\epsilon}_x$. From Eqn.(1), the emittance measurement reduces to the measurement of the second order moments of the distribution.

We will use the JLab FEL photoinjector as a basis for numerical computations, it is worthwhile to recall in Tab. 1 the principal beam parameters at the two locations we wish to measure the transverse emittance. A more complete description of the injector is found in Ref. [5] and references therein. Our goal is to measure a normalized emittance

parameter	Location #1	Location #2
$\bar{\epsilon}_x^n$ (mm-mrad)	6.6	8.8
$\sigma_{x'}$ (mrad)	0.6	0.3
σ_x (mm)	2.3	1.9
$\bar{\epsilon}_y^n$ (mm-mrad)	6.0	6.2
$\sigma_{y'}$ (mrad)	0.5	0.2
σ_y (mm)	2.3	1.4

Table 1: Beam parameters predicted by PARMELA for the baseline design injector (Q=135 pC); the total energy is 10 MeV.

ranging from 4 to 20 mm-mrad, with the nominal emittance being approximately 7 mm-mrad.

2 OTR-BASED TECHNIQUE

When a beam of charged particles has the electric permittivity of its environment changed, it emits transition radiation (TR). The use of this radiation for beam diagnostic purposes has become popular in recent years: in electron accelerators such radiation is generated by intercepting the beam with very thin metallic foils and observing the backward TR. For a single electron the TR angular distribution given by [6]:

$$\frac{d^2 I}{d\omega d\Omega}(\theta, \gamma) = \frac{e^2 \beta^3}{\pi^2 c} R \frac{\sin^2 \theta}{(1 - \beta^2 \cos^2 \theta)^2} \quad (2)$$

where $\beta^2 = 1 - 1/\gamma^2$ (γ being the usual Lorentz factor) and R is the reflection coefficient of the foil ($R \simeq 1$ for a metallic foil at optical wavelengths). The generated TR can be used to measure the rms beam spot size by computing the quantity:

$$\langle x^2 \rangle = \frac{\int x^2 I(x, y) dx dy}{\int I(x, y) dx dy} \quad (3)$$

* Work supported by the US-DOE contract #DE-AC05-84ER40150, the Office of Naval Research, the Commonwealth of Virginia, and the Laser Processing Consortium.

where $I(x, y)$ is the two-dimensional density of the TR image on the foil. The beam divergence can be inferred from the observation of the TR angular distribution since it corresponds to the convolution of the TR intrinsic angular distribution with the beam angular density $P(x')$:

$$\frac{d^2 I}{d\omega d\Omega}(\theta, \gamma) = \int \frac{d^2 I(\theta - \alpha, \gamma)}{d\omega d\Omega} P(\alpha) d\alpha \quad (4)$$

Hence if the upstream magnetic optics is properly tuned to achieve a waist at the location of the TR screen, the emittance can be estimated by computing the quantity:

$$\epsilon_x = [\langle x^2 \rangle \langle x'^2 \rangle]^{1/2} \quad (5)$$

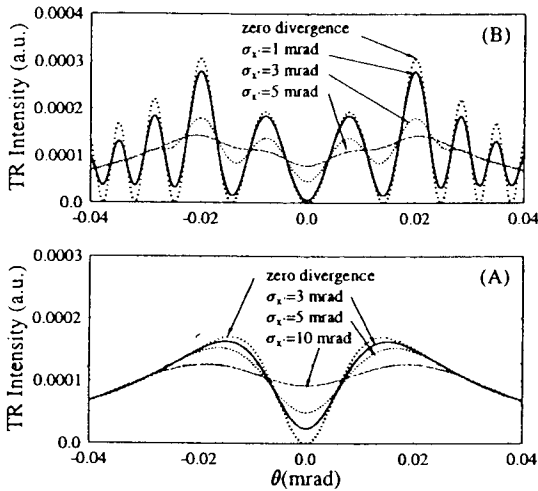


Figure 1: Dependence of the single foil TR angular distribution (A) and interferometric TR angular distribution (B) for different beam divergences. For case (B), the wavelength of observation is $\lambda = 500$ nm and the foil space is $L \simeq \lambda\gamma^2$.

Figure 1(A) shows the effect of beam divergence on the TR angular distribution for a beam of 38 MeV (at 10 MeV the effect is not very pronounced). The use of fitting to obtain the divergence (and subsequent emittance) measurement has been successfully implemented in several facilities [7, 8]: the experimental TR angular distribution is fitted with two parameters (energy and divergence). The minimum rms beam divergence that can be experimentally resolved is approximately $x' \simeq 0.15\gamma^{-1}$ [8]. Such a method was quickly replaced by a more precise method based on the Wartski [6] two-foil interferometer: instead of directly detecting the backward TR emitted from the foil, the interference pattern between the forward TR emitted as the beam crosses an upstream foil and the backward TR of a second foil is analyzed. The distance between the two foils must be larger than the far-field parameter $\Lambda = \lambda\gamma^2$ where λ is the wavelength at which the interference pattern is ob-

served. In this case Eqn.(2) takes the form:

$$\frac{d^2 I}{d\omega d\Omega} \propto \frac{\sin^2 \theta}{(1 - \beta^2 \cos^2 \theta)^2} \sin^2 \left(\frac{\pi L}{\lambda} (1 - \beta \cos \theta) \right) \quad (6)$$

Simulations of the interference patterns for different beam divergences are presented in Fig. 1(B). In these numerical computations, we have simply convolved the Eqn.(6) with the beam angular distribution that is assumed to be gaussian, the beam energy being 38 MeV. The effect of increasing the divergence results in a blurring of the angular distribution. The previous remarks also pertains: for a 10 MeV beam we cannot resolve beam divergence comparable to the one expected in the JLab FEL injector (approximately 0.2 to 0.6 mrad). As in the single foil case, the experimentally obtained interference pattern is fitted using two parameters (divergence and energy) from which the divergence is computed, providing an emittance using Eqn.(5). The advantage of this method comes from the oscillations that occur at positions depending on energy, it generally gives more accurate fits compared to the single foil method. Also, because the distribution is dependent on the wavelength of observation and the distance between the two foils, it is possible, using these dependencies, to “tune” the interferometer in order to increase the accuracy of the measurement. TR-based methods are very attractive because of their simplicity, generally two CCD detectors and a beam splitter are needed. Unfortunately they have a number of drawbacks: Firstly, it is necessary to locate such devices at a beam envelope waist or to tune the upstream optics to achieve such waist. Secondly in the case of the two-foils scheme, the first foil used to emit forward OTR inevitably increases the beam divergence due to multiple scattering. This is especially important for low energy beams; typically this method is suitable only for a beam whose divergence $\sigma_{x'}$ and energy γ satisfy a relation of the type $\sigma_{x'} \gg f(Z, \Omega)/(mc^2\gamma)$ where f is a function of the foil atomic number Z and the mean number of collisions Ω , and can be estimated from results discussed in Ref.[9]. Also, both of these methods are difficult to apply to measure the emittance of a space-charge-dominated beam, e.g., as it is often the case for high-brightness injectors. Indeed, they can be used provided the beam sizes $\sigma_{x,y}$ at the horizontal waist satisfy the relation (the same equation obtains in the vertical plane replacing x subscript by y):

$$2K\sigma_x^2 / \left[\tilde{\epsilon}_x^2 \left(1 + \frac{\sigma_y}{\sigma_x} \right) \right] \ll 1 \quad (7)$$

where $K = 2I_p/((\beta\gamma)^3 I_A)$ is the normalized perveance (I_p and I_A are respectively the peak and Alfvén current). Successful use of OTR interferometry has been reported by several groups, with an extensive study performed on the BOEING FEL facility [10]. A measurement of divergence of approximately 100 μ rad for 650 MeV beam is planned on the APS undulator test line [11].

3 TRACE SPACE SAMPLING METHODS

Trace space sampling techniques are widely used to characterize the trace space density with high precision. The most popular example is the “slit and collector” method that has been used by several teams to characterize guns. Though it does not provide an on-line measurement, variants of this technique have been used to perform single shot measurements. In such methods a single slit is replaced by an interceptive mask where several apertures are bored. The different methods commonly in use differ in essentially two ways: in the shape of the sampling apertures but also in the type of “collector” device used to observe the beamlet profiles (fluorescent screens, optical transition radiation (OTR), wire scanner). The principle of the trace

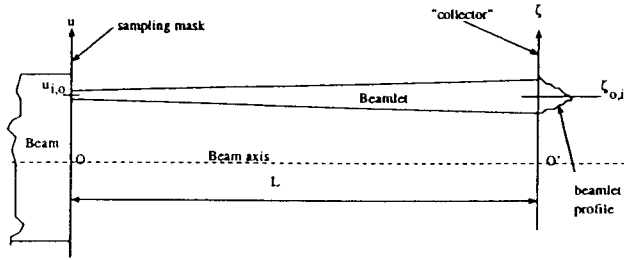


Figure 2: Basis of trace space sampling technique.

space sampling is sketched in Fig. 2, where we consider the one-dimensional case: the sampling aperture is assumed to have a zero-extension along the coordinate axis u . The generated beamlet strikes the collector device after propagating through a drift of length L . For the generated beamlet, the second order moments are $\langle u_{0,i}^2 \rangle$, $\langle ((\zeta - \zeta_{0,i})/L)^2 \rangle$ and $u_{0,i} \langle (\zeta - \zeta_{0,i})/L \rangle$. For a set of n beamlets, the second order moments are given by the relations:

$$\langle u^2 \rangle = \left\langle \sum_{i=1}^n u_{0,i}^2 \right\rangle, \quad \langle u'^2 \rangle = \left\langle \sum_{i=1}^n \frac{(\zeta - \zeta_{0,i})^2}{L^2} \right\rangle \quad (8)$$

$$\langle uu' \rangle = \left\langle \sum_{i=1}^n u_{0,i} \frac{(\zeta - \zeta_{0,i})}{L^2} \right\rangle$$

Using the set of Eqns.(8) and Eqn.(1), we can estimate the beam parameters of the incident beam.

In the case of on-line measurement, OTR screens or fluorescent screens are commonly used. The latter are generally preferred because they are very sensitive, but offer worse resolution, and care must be taken to use them in their linear response range. Also the persistence of such screens can be problematic for single-shot measurement. OTR screens, on the other hand, provide high resolution but the photon/electron conversion is very small (typically $1/\alpha$, α being the fine structure constant) and special attention must be directed toward maximizing the S/N ratio by reducing the background noise.

Another task common to all these methods is the choice of mask material and thickness. If we restrict our discussion to uncooled systems, a high thermal conductivity material should be chosen to efficiently dissipate the beam deposited power. Also thermal bridges toward the exterior of the vacuum chamber should be used. Thermal analysis of the mask with the beam deposited power is necessary especially when OTR screens are used as collectors, since they require the highest possible average current to maximize the S/N ratio. Copper is a good choice because it offers a relatively good emissivity and therefore part of the deposited power is dissipated via black body type radiation. Other materials such as stainless steel are generally employed when the collector is a fluorescent screen. The deposited power may be reduced by choosing a proper beam temporal structure (micropulse frequency, and macropulse width and frequency) provided multi-bunch effects are not significant, a true assumption in the case of the JLab FEL where the bunches are separated by 8.03 m.

The thickness of the mask is a compromise between the S/N ratio on the collector and edge scattering of the electron on the aperture edge. Ideally, it is desirable to have a thickness that is of the order of the stopping thickness $\gamma mc^2/(dE/dx)$ where dE/dx is the energy loss per unit of pathlength in the material. On the other hand, if the thickness is too large, particles can scatter on the aperture edges and thereby change their divergences [15]. The thickness can be determined by considering the rms scattering angle given by the Molière theory [12]:

$$[\langle \theta_{\text{scat}}^2 \rangle]^{1/2} = \frac{13.6}{\beta c p} z \sqrt{l/X_0} [1 + 0.038 \ln(l/X_0)] \quad (9)$$

where p the momentum in MeV/c, z is the charge number, and l/X_0 is the mask thickness in units of radiation length X_0 . Using the previous relation we can determine the thickness of the mask l so that the rms scattering angle is much larger than the angle subtended by the collector. In such cases, the scattered particles will contribute as a uniform background without biasing the beamlet pattern and one avoids erroneous values for the beam parameters. We have investigated the importance of edge scattering by using the PARMELA-generated phase space for the JLab FEL and numerically retracing each macroparticle through apertures. We found that in the case of the JLab FEL nominal emittance and divergence at the location where we perform the measurements, less than 5% of the particles were interacting with the edge even in the presence of a slight misalignment of the mask axis with respect to the beam axis of the order of 1 mrad. Therefore this latter effect is assumed to be insignificant, and no special care such as aperture tapering was considered for the case of the JLab FEL.

By a proper choice of aperture size, trace-space sampling allows the measurement of space-charge-dominated beams. The aperture size should be determined so that the space-charge contribution to the beamlets envelope equa-

tion is much smaller than the emittance contribution using Eqn.(7). In such cases, the beam parameters can be inferred using Eqn.(8) since the beamlets are emittance dominated and their behaviour is governed by linear optics. If w_x and w_y are the characteristic sizes of the aperture, they should fulfill the relation:

$$\frac{K w_{x,y}^2}{6(\bar{\epsilon}_{x,y})^2 \left(1 + \frac{w_{y,z}}{w_{x,y}}\right)} \ll 1 \quad (10)$$

where the coefficients are as defined in Eqn.(7).

The separation between the apertures center d and the distance between the mask and the collector L depend on the beam size and beam divergence. By requiring the resolution to be the same in position and divergence a relation between the aperture spacing and distance can be derived:

$$\sigma_{x,y}/d \simeq L \frac{\sigma'_{x,y}}{r} \quad (11)$$

where r is the resolution of the detector. On the other hand, to ensure the beamlets do not overlap we must have:

$$4\sigma'_{x,y}L < d \quad (12)$$

Using the two latter equations we find for a given set of beam parameters all the geometric parameters of the mask.

The acquisition system requires a frame grabber to digitize the analog signal from the CCD detector. In the case of JLab FEL, we use a DATACUBE digitizer that operates under the EPICS environment. The digitized data are directly reduced on the same CPU as the one controlling the digitizer using the VxWorks language, and only results (values of beam parameters, trace-space plot) are broadcast on the network. These results can be accessed from any X-window stations using an EPICS-based screen [17].

3.1 The pepper pot method

In the pepper pot technique [13, 14], the mask consists of a matrix of generally circular apertures. The beamlets in the collector plane are given by:

$$I_{i,j}(x', y') \simeq \rho_4(x_i, x'; y_j, y') \delta S \quad (13)$$

where δS is the area of the apertures. The projection on the x -axis, i.e., summing on y_j and integrating on y' is:

$$P_i(x') \propto \rho_2(x_i, x') \delta S \quad (14)$$

From $P_i(x')$ we can compute the second order moments of the $x - x'$ trace space distribution $\rho_2(x, x')$ and deduce the beam parameters. In fact, the pepper pot method allows one to study coupling between the horizontal and vertical trace space; using Eqn.(13) the coupled second order moments $\langle xy \rangle$, $\langle x'y \rangle$, $\langle xy' \rangle$ and $\langle x'y' \rangle$ can be computed. Hence the rms hyper-transverse emittance can be estimated. Though this method can provide much information on the transverse trace space, it is difficult to get a decent signal by

using an OTR screen as collector. In the JLab FEL case, the required aperture radius would be approximately $40 \mu\text{m}$ which implies that the average beamlet charge will be less than 6 pC, not a large enough number to produce enough OTR photons than can be detected with conventional CCD detectors.

3.2 The multislit method

In the case of the Jefferson Lab FEL, we have opted for this method which offers the same features of the pepper pot technique (without the possibility of measuring the hyper-emittance) with the advantage of providing much more signal. Its principal disadvantage is that the horizontal and vertical phase space measurements have to be performed separately and therefore the method requires two masks. Practically we have addressed this issue by mounting two sets of slits on the same mask, mounted on a two position air cylinder so that horizontal and vertical measurements can be performed one after the other. In the horizontal plane, the beamlets pattern generated by vertical slits centered at x_i is given by:

$$P_i(x') \propto w \rho_2(x_i, x') \quad (15)$$

where w is the slit width. When writing Eqn.(15) it is implicitly assumed that the slits are infinitely narrow. If such an approximation cannot be made; one should use formulae derived in Ref. [18]. For the JLab FEL we have carefully optimized the slits geometric parameters using PARMELA, taking as starting point numerical values computed from the previous discussion. For the

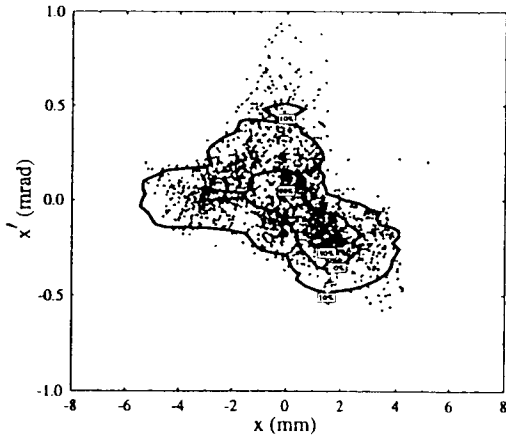


Figure 3: Simulation of emittance measurement with the multislit mask. The dots are macroparticles generated with PARMELA. The iso-contours are computed from the retrieved phase space after simulating the emittance measurement using the PARMELA distribution.

baseline injector the optimized values for the multislit mask are: (1) a slit spacing of 1.5 mm, (2) a slit width of $0.75 \mu\text{m}$, and (3) a mask thickness of 5 mm. In our

case the distance between the mask and the OTR screen was set by mechanical constraints to 620 mm. With such parameters, a systematic error in the 10% range for the nominal emittance was found. In Tab. 2 we compare the PARMELA simulated emittance with the computed emittance simulating the emittance measurement, the initial and retrieved trace space are plotted in Fig. 3. Systematic errors are numerically estimated using errors propagated with the anticipated distribution and include finite slit width effects. Other source of error such as remanent space-charge in the beamlets, space-charge field perturbation due to the slits have been considered and were found to be negligible. However, finite sampling error is a concern and should be reduced below 10% provided that 5 slits, at least, are illuminated by the incident beam. The first tests were performed in the

$\bar{\epsilon}_x^n$ _{parmela}	$\bar{\epsilon}_x^n$ _{retrieved}	$\Delta\bar{\epsilon}/\bar{\epsilon}\%$ (a)	$\Delta\bar{\epsilon}/\bar{\epsilon}\%$ (b)
8.094	8.077	0.2	9.9
3.947	4.014	1.7	19.9
24.282	23.016	5.2	2.7

Table 2: Simulation of emittance measurement for different emittance, after slit optimization. The quantity $\Delta\bar{\epsilon}/\bar{\epsilon}$ (a) is just a measure of the relative difference between the nominal and retrieved emittance while the quantity $\Delta\bar{\epsilon}/\bar{\epsilon}$ (b) represents the systematic error estimate.

JLab Injector Test Stand. Because of low energy, 350 keV, we were using, as collector, a fluorescent instead of an OTR screen. We compare the multislit method with the "slit and collector" apparatus [16, 17] and agreement at the 15% level was observed. Recent measurements performed in the JLab FEL operating at 60 pC (therefore with a lower beam emittance) are presented in Fig. 4. The emittance typically measured is approximately 6 mm-mrad which is somewhat larger than PARMELA prediction for this charge. Also because the beam divergence and size are different from those expected at 135 pC (the charge for which the mask has been optimized), the number of generated beamlets is only 4-5. This is a disadvantage of single shot phase space sampling method; they have to be designed for specific parameters and have a limited dynamic range. Multislit mask devices have been in use for several years in the UCLA group [19] to characterize a high brightness electron injector and in the CERN heavy ion injector to measure emittance of heavy ions beams [20].

The authors are indebted to the FEL commissioning team for support and operation of the machine.

4 REFERENCES

[1] C. Lejeune, et al., *Advances in Electronics and Electron devices, Supp.* **13A**, 159-259 (1980)
 [2] F. Sacherer, *IEEE Tran. Nuc. Sci.* **NS 18** 1105-1107

[3] P. Lapostolle, CERN rep. CERN/DI-70-36 (1970)
 [4] J.D. Lawson, et al., *Part. Accel.* **5**, 61 (1973)
 [5] P. Piot, et al., *proc of the Euro. Part. Acc. Conf.'98*, (Stockholm, Sweden)
 [6] L. Wartsky, PhD Thesis, Université Paris Sud (unpublished)
 [7] X. K. Maruyama, et al., *Nucl. Inst. Meth.* **A272**, 237-240 (1987)
 [8] R. Fiorito et al., *AIP Conf. Proc.* **319**, 21-37 (1994)
 [9] P. Piot, et al., *AIP Conf. Proc.* **390**, 298-305 (1996)
 [10] D. Rule, et al., *Nucl. Inst. Meth.* **A296**, 739-743 (1990)
 [11] A. H. Lumpkin et al., *Nucl. Inst. Meth.* **A341**, 417-421 (1994)
 [12] D. E. Groom et al., *Eur. Phys. Journ. C* **3** Num. 1-4, 144 151 (1998)
 [13] A. Vignati, et al., *Nucl. Inst. Meth.* **B66**, 503-507 (1992)
 [14] Y. Yamazaki, et al., *Nucl. Inst. Meth.* **A322**, 139-145 (1992)
 [15] E. D. Courant, *Rev. Sci. Instr.* **22** num 12, 1003-1005 (1951)
 [16] P. Piot, et al., *proc of the Part. Acc. Conf.'97* (Vancouver, Canada)
 [17] J. Song, et al., *Nucl. Inst. Meth.* **A407**, 343-349 (1998)
 [18] M. J. Rhee, et al., *Rev. Sci. Instrum.* **62**(6), 1468-1470 (1991)
 [19] S.C. Hartman, et al., *proc of the Part. Acc. Conf.'93*, 561-563 (1993); S.C. Hartman PhD Thesis, UCLA (unpublished)
 [20] M. Crescenti, et al., *Proc. of the Diag. Inst. Part. Acc.*, 66-68 (1995)

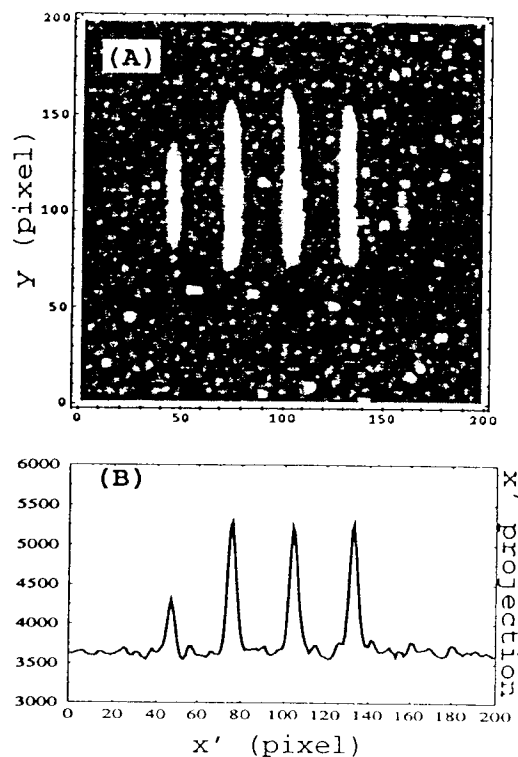


Figure 4: Typical beamlet pattern from a multislit mask. OTR image of the beamlets (A) and projection along the y-axis (B).